DIASCoPE: Directly integrated acoustic system combined with pressure experiments—A new method for fast acoustic velocity measurements at high pressure

Matthew L. Whitaker,[a] Kenneth J. Baldwin, and William R. Huebsch
Mineral Physics Institute, Stony Brook University, Stony Brook, NewYork 11794-2100, USA

(Received 15 June 2016; accepted 15 February 2017; published online 9 March 2017)

A new experimental system to measure elastic wave velocities in samples *in situ* under extreme conditions of pressure and temperature in a multi-anvil apparatus has been installed at Beamline 6-BM-B of the Advanced Photon Source at Argonne National Laboratory. This system allows for measurement of acoustic velocities via ultrasonic interferometry, and makes use of the synchrotron beam to measure sample densities via X-ray diffraction and sample lengths using X-radiographic imaging. This system is fully integrated into the automated software controls of the beamline and is capable of collecting robust data on elastic wave travel times in less than 1 s, which is an improvement of more than one to two orders of magnitude over existing systems. Moreover, this fast data collection time has been shown to have no effect on the obtained travel time results. This allows for more careful study of time-dependent phenomena with tighter snapshots in time of processes that would otherwise be lost or averaged out in other acoustic measurement systems. *Published by AIP Publishing.* [http://dx.doi.org/10.1063/1.4977596]

I. INTRODUCTION

Advances in *in situ* experimental techniques using synchrotron radiation at extreme conditions of pressure and temperature have helped to provide answers to fundamental questions that were previously unattainable. In particular, synchrotron-based ultrasonic interferometry measurements have proven to be especially important in determining acoustic velocities and thermoelastic properties of materials at high pressures and temperatures. These experiments have proven to be particularly useful in the earth sciences, where determining the elastic properties of minerals is critical to understanding and interpreting seismic velocity profiles of the Earth's interior (see reviews in Refs. 1 and 2).

The measurement of acoustic velocities using ultrasonic interferometry is done by simply dividing the measured sample length by the observed travel time of the acoustic wave and has been used in high pressure laboratory experiments for over fifty years (i.e., Refs. 3–11). The modern methodology of coupling these ultrasonic measurements with synchrotron X-ray measurements of sample length (L) and volume (V) was pioneered by researchers at Stony Brook University (see Ref. 12) working at Beamline X17B2 of the National Synchrotron Light Source (NSLS). This experimental methodology allowed for direct simultaneous adiabatic bulk (K_S) and shear (G) modulus measurement in the sample *in situ* as a function of pressure (P) and temperature (T).

Similar experimental systems have since been installed at other synchrotron facilities around the world[13–15] and used to make high pressure measurements and derive accurate P-V-(T)-K_S-G equations of state on a variety of Earth materials and beyond (i.e., Refs. 16–30, and reviews in Refs. 1 and 2). However, due to relatively slow data collection times, it has been difficult to measure the effects of processes as they occur, such as melting or phase transformations, and instead the measurement is made on the end product of these processes. The new system described here is an important step toward addressing this problem.

DIASCoPE (Directly Integrated Acoustic System Combined with Pressure Experiments) is a new type of on-board ultrasonic acoustic velocity measurement system that has cut acoustic wave travel time measurements by one to two orders of magnitude. With this new system P- and S-wave travel times can be measured in samples at extreme conditions in less than 1 s. Moreover, the system has been fully integrated with the multi-anvil apparatus and the EPICS control system at newly commissioned beamline 6-BM-B of the Advanced Photon Source (APS), allowing for greater ease of control and full automation of experimental data collection. In this paper, we demonstrate the concept and execution of the system, how it is different from previous experimental setups, and show that the data collected in such short time scales are robust.

II. ULTRASONIC EXPERIMENTAL METHODOLOGY

This new system for measuring acoustic wave velocities *in situ* at high pressures and high temperatures has been installed at Beamline 6-BM-B at APS. This beamline houses a 250-ton hydraulic multi-anvil press (SAM85) equipped with a DDIA pressure module. Figure 1 shows a schematic diagram of the experimental setup and the different types of data that are collected during an experiment. An example of the standard cell assembly used in these ultrasonic experiments is shown in Figure 1(a). The cubic pressure medium can be made from several different materials; the three shown here were the

[a]Author to whom correspondence should be addressed. Electronic mail: matthew.whitaker@stonybrook.edu

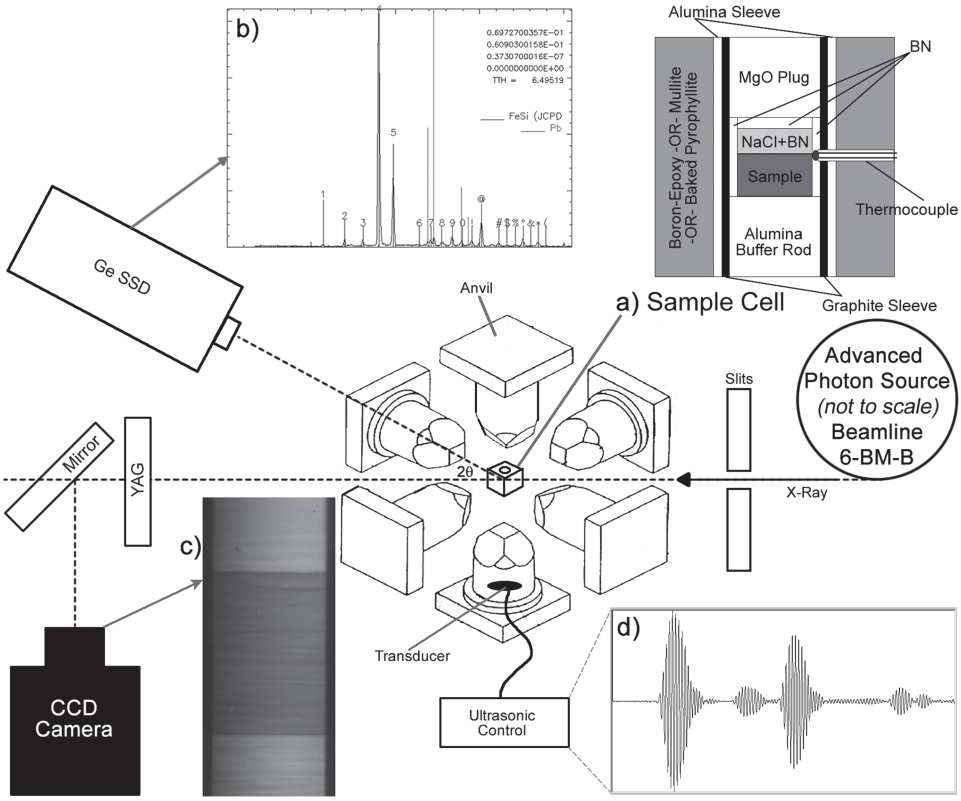

FIG. 1. Outline of the DIASCoPE experimental setup at beamline 6-BM-B at APS. (a) Cell assembly—schematic diagram of the standard cell assembly used for acoustic measurement experiments. A 1 μm-thick disc of Au foil is placed above and below the sample and at the bottom of the buffer rod to smooth all contact surfaces and act as a marker in the X-radiographic images. (b) Sample energy dispersive X-ray diffraction pattern collected during an experiment with indexed peak positions and Pb fluorescence lines shown for reference. (c) Sample X-radiographic image collected during experiment. (d) Ultrasonic interferometer allows for the collection of both P and S wave data as a function of pressure and temperature.

ones used during the testing and commissioning of the DIASCoPE system. The graphite sleeve acts as the resistive heater during the experiment. The NaCl mixture behind the sample and the surrounding BN sleeve provide a pseudohydrostatic sample environment. Two different salt mixtures were used in the commissioning experiments: NaCl:BN (10:1 by weight) and NaCl:BN+Au (4:1 by volume +10 wt.% Au). The NaCl and Au have well-established equations of state (i.e., Refs. 31 and 32) and thus also serve as pressure standards during the experiment.

Energy dispersive X-ray diffraction patterns (Fig. 1(b)) for the sample and the pressure calibrants are collected by solid state germanium detectors. Adjustable tungsten slits upstream from the sample can collimate the incident X-ray beam to anything from 5×5 mm to 25×25 μm; typically for diffraction a beam size of 100×100 μm is used. Though only a single detector is shown in the schematic for simplicity, beamline 6-BM-B actually has a 10-element detector array with the individual elements oriented in a circular array. A series of two conical slits then fixes the 2-theta of the diffracted X-ray beam at 6.50° for all ten detector elements. Refinement of the diffraction patterns yields the unit cell volume and thus the density (ρ) of the sample as well as its stress state as a function of pressure and temperature.

For X-radiographic imaging, the incident slits are opened wide (4 mm vertical, 3 mm horizontal) to allow the entire sample area to be bathed in X-rays. The X-ray beam passes through the cell assembly and then through a single-crystal YAG scintillator. This YAG fluoresces and the visible light is reflected off of a mirror and collected by a Prosilica CCD camera which can save snapshot images of the cell assembly as a function of pressure and temperature (Fig. 1(c)). Differences in linear X-ray absorption coefficients and travel lengths and the densities of the materials in the cell assembly lead to brightness contrasts which are used to identify the sample and monitor its length during the experiment. By determining sample length in pixels at the end of the experiment when the press is opened and comparing it to the precisely measured absolute length of the sample after the experiment, the pixel-to-length ratio can be calibrated. This allows for the determination of the absolute length (L) of the sample as a function of P and T with a 0.2%-0.4% precision.[12]

Measurement of elastic wave velocities is conducted via ultrasonic interferometry utilizing a dual-mode 10° Y-cut $LiNbO_3$ piezoelectric transducer (Fig. 1(d)). This type of transducer is capable of generating and receiving frequencies from ~20 to 70 MHz which allows for the collection of both compressional (P) and shear (S) waves during the same experiment, with a standard deviation of ~0.2-0.5 ns. To ensure minimal loss of acoustic energy at the interfaces between materials, all surfaces along the acoustic travel path were polished with 1 μm diamond paste to be perfectly flat and parallel within 0.05°. As shown in Figure 2, this includes both the bottom and top surfaces of the WC anvil on which the transducer was mounted, and both sides of the buffer rod and sample. A 1 μm-thick disc of gold foil is placed between the anvil and buffer rod, and between the buffer rod and sample to enhance the coupling between the surfaces. These foil discs also serve as markers for measuring length in X-radiographic images.

The transducer has different resonant frequencies for compressional and shear waves, and these frequencies are determined empirically during the experiment by optimizing the

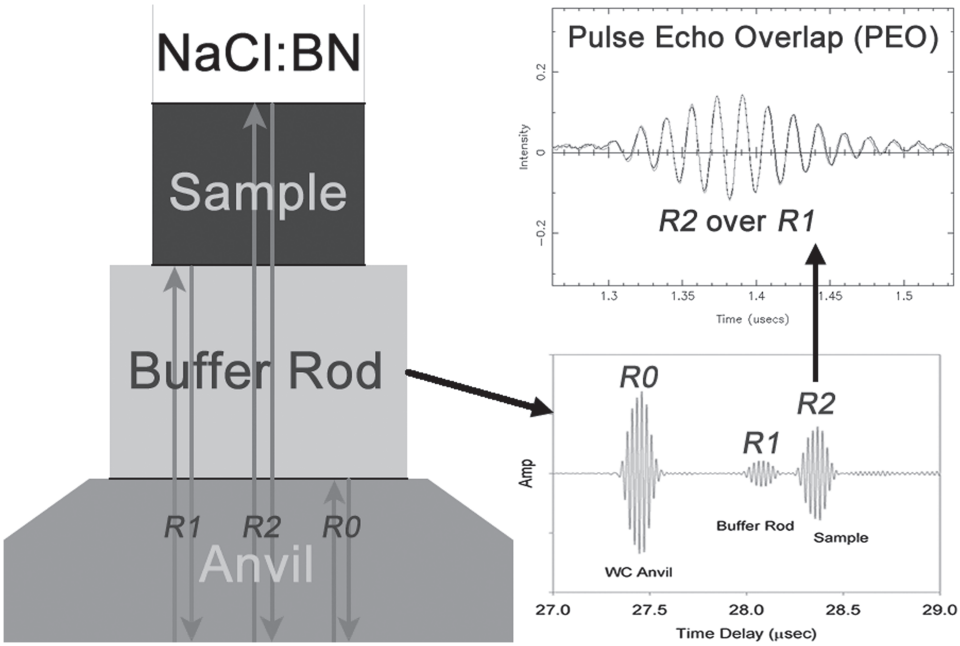

FIG. 2. Outline of acoustic wave travel path during experiments. The acoustic wave is sent into the cell assembly by a transducer on the back of the anvil and this transducer then records the reflection of these acoustic waves from the anvil surface ($R0$), the interface between the buffer rod and sample ($R1$), and the back side of the sample ($R2$). The two-way travel time of the acoustic wave in the sample is then determined via the Pulse Echo Overlap (PEO) technique by overlaying $R2$ over $R1$ and measuring the time offset.

signal-to-noise ratio in the ultrasonic data. Once optimum frequencies are determined, the acoustic response of the cell assembly is recorded at these frequencies. For the transducer used in this study, the optimum frequency for compressional waves is ~60 MHz, while for shear waves it is ~35 MHz. The system collects 1024 acquisitions and adds them together to maximize the signal-to-noise ratio. These data are then analyzed using the Pulse Echo Overlap (PEO) method (Fig. 2), where acoustic wave travel times in the sample are measured by determining the time offset when the reflection from the back surface of the sample ($R2$) is directly overlain and visually/mathematically matched to the reflection from the back side of the buffer rod ($R1$). The results of this analysis yield the two-way travel time of compressional (t_P) and shear (t_S) waves in the sample as a function of pressure and temperature.

The data collected during the experiment can now be used to derive an accurate P-V-(T)-K_S-G equation of state for the sample being studied. The X-ray diffraction data give the volume (V) and density (ρ) of the sample, while the X-radiographic image yields the sample length (L). The ultrasonic data give the two-way travel times of elastic waves in the sample (t_P and t_S). Compressional wave velocity $V_P = 2L/t_P$ and shear wave velocity $V_S = 2L/t_S$. Since these are all measured parameters, adiabatic bulk ($K_S = \rho V_P^2 - 4G/3$) and shear ($G = \rho V_S^2$) moduli of the sample have been determined for each set of data collected as a function of pressure (P) and temperature (T). These data can then be fit simultaneously to third-order finite-strain equations[33] to obtain the zero-pressure, room-temperature elastic bulk, and shear moduli and their respective pressure and temperature derivatives (see Refs. 17, 19, and 28 for examples).

III. DIASCoPE SPECIFICATIONS

The above is a general overview of how most high pressure *in situ* ultrasonic experiments work and the types of data and results that can be obtained from them, including DIASCoPE experiments. However, DIASCoPE is different from all other high pressure ultrasonic experimental systems because of two main factors: (1) the speed at which it conducts and collects acoustic wave velocity measurements, and; (2) it is fully integrated into the beamline controls and data acquisition software, which allows for more precise control over the experiment and even automation of experimental protocols.

The Ultrasonic Control shown in Figure 1(d) is explained in detail in block diagram form in Figure 3. A simple Wavetek pulse generator feeds directly into the digital oscilloscope and provides a constant (adjustable) time base for the entire system. This pulse generator defines the frequency at which the system can be triggered to send pulses and receive the measured travel time data and therefore the time it takes to collect the ultrasonic data. For example, if an experiment is set to collect 1024 acquisitions, and this time base is set to 1 kHz, it takes 1 s to complete and record the full measurement. However, if the time base is set to 250 Hz, it will take 4 s to complete the measurement. It was empirically determined that selecting a single waveform collection time of less than 1 ms (>1 kHz on the time base) resulted in data loss from the digital

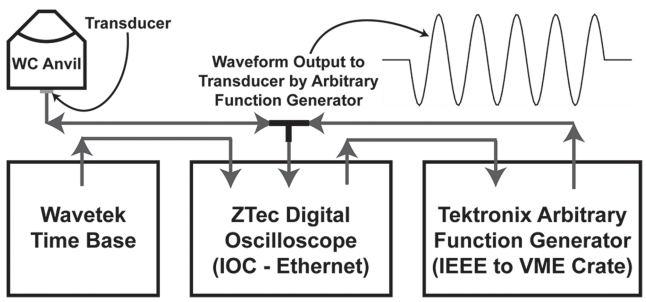

FIG. 3. Block diagram of communications for the ultrasonic interferometry measurements in the DIASCoPE system. Path of communications shown by arrows. The system interfaces directly with EPICS allowing for integration into the beamline control system.

oscilloscope. Therefore, the system has been optimized to run using a 1 kHz time base for data collection. Since the acoustic response of the cell assembly is recorded over a period of 40-50 μs, the maximum rate at which the acquisitions could be collected is ~20-25 kHz. This rate is the theoretical maximum, not accounting for overhead that must be accounted for in the form of delays between acquisitions and times associated with data output and file writing. Therefore, this electronics-based limitation of 1 kHz is very near the theoretical limitation for data collection in these experiments.

The generator used to create the input signals in DIASCoPE is a Tektronix AFG3251C Arbitrary Function Generator. This generator is triggered by the oscilloscope and sends its signal, usually a multi-cycle sine wave in the case of these experiments (see Fig. 3), to the transducer which then sends the sound waves into the sample and returns the acoustic response of the cell to the oscilloscope. The generator offers fine frequency control down to the Hz which allows for precise control of the input signal.

The oscilloscope in the DIASCoPE system is a ZTec ZT4611-E model digital oscilloscope. This is the critical piece of equipment that allows for such fast measurements of acoustic velocities. In most digital oscilloscopes the data for each acquisition are dumped from the scope to the hard drive of the controller and summed as each new acquisition is collected. Depending on the software used and quality of hardware in the scope, this can be a serious time sink. In DIASCoPE, we have been able to bypass that process by doing the collection and summing of multiple acquisitions directly in the oscilloscope hardware itself before outputting the final summed waveform for data retrieval. This has cut data collection time for 1024 acquisitions from 30 to 180 s down to 1 s—an improvement of more than 1-2 orders of magnitude.

The Tektronix arbitrary function generator connects via an IEEE-488 cable to the General Purpose Interface Bus (GPIB) carrier in the VME crate that runs the beamline control system. The ZTec oscilloscope communicates via an Ethernet connection and has EPICS drivers built in to the control system, so it acts as its own input/output controller (IOC). Both the generator and the oscilloscope are therefore directly accessible via EPICS beamline controls. These controls give direct real-time control of the frequency and cycles of the signal put out by the generator, which allows for switching the signal between P- and S-wave frequencies in milliseconds. We also have the ability to control data acquisition, output, and

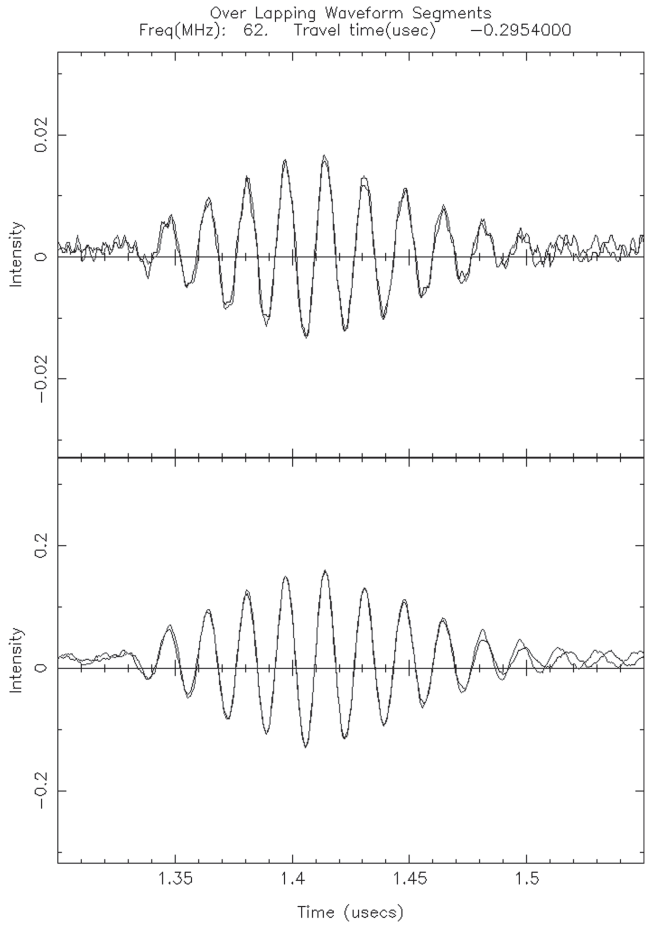

FIG. 4. Plot showing P-wave travel time determination using the Pulse Echo Overlap (PEO) technique. Reference sample is a cylinder of dense polycrystalline fayalite 2.0 mm in diameter and ~1 mm in length. Signal was collected in the D-DIA at 35 ton ram load (~5 GPa) and room temperatrue. Input signal was 5 cycles of a 62 MHz sine wave. Top panel shows 1024 summed acquisitions collected in 1 s. Bottom panel shows 10 240 summed acquisitions collected over a 28 s period (1024 acquisitions in 1 s with a 2-s delay between acquisition steps).

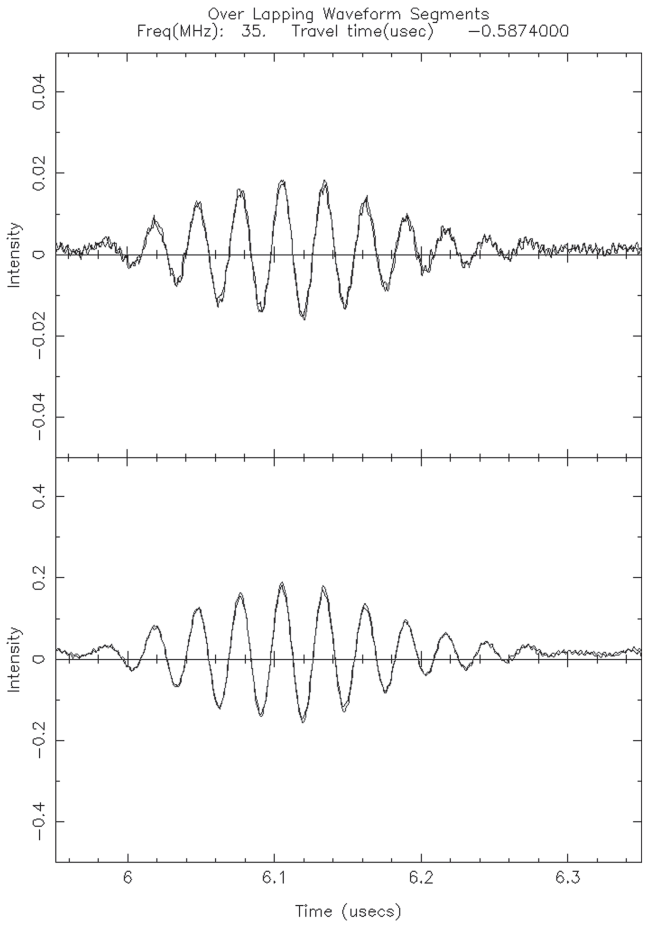

FIG. 5. Plot showing S-wave travel time determination using the Pulse Echo Overlap (PEO) technique. Input signal was 5 cycles of a 35 MHz sine wave. Panels are organized as in Figure 4.

visualization utilizing the native EPICS controls in the oscilloscope. This allows for a single control overlay to accommodate collection of X-ray diffraction data, X-radiographic images, and ultrasonic interferometry measurements. In addition to the speed with which DIASCoPE can make these acoustic velocity measurements, this direct access and automated control of the entire system set it apart from any other similar acoustic measurement system presently available.

IV. DATA COMPARISON

The main questions regarding DIASCoPE during the commissioning and testing phase revolved around the quality and robustness of the data collected in such short time periods. Would the data be clear and unambiguous enough to determine reliable acoustic wave travel times in the experimental sample? How does the data collected with DIASCoPE compare to the data collected over a longer time period? The data collected during commissioning have provided an answer to these concerns.

Figure 4 shows the P-wave travel time determination in a reference sample using the Pulse Echo Overlap (PEO) technique, overlaying the sample reflection with the buffer rod reflection (R2 over R1 in Figure 2). The top and bottom panels are scaled to be identical. The top panel shows the PEO results for a single waveform of 1024 summed acquisitions collected in 1 s. The bottom panel shows the PEO results for 10 summed waveforms of 1024 acquisitions collected in 1 s with a 2-s delay time between waveform collections (10 240 acquisitions). This means the data were collected over a period of 28 s, which is similar to the fastest collection times available using other multi-anvil-based ultrasonic systems.

There are two major things that are important to note here that speak directly to the concerns raised at the beginning of this section. First, it is clear that the ultrasonic data collected in 1 s, as shown in the top panel of Figure 4, are robust enough for a precise determination of acoustic wave travel time in the experimental sample. Second, the extended data collection procedure over a longer time period did not alter the travel time determined via PEO of the waveform data output. The travel time for both datasets came out identical and is shown in the header lines of Figure 4. While it is true that the signal to noise ratio is significantly improved in the bottom panel of Figure 4 as compared to the top, which would be expected considering there were ten times as many acquisitions in the final waveform output, this had no effect on the reflection positions or the results obtained during data analysis. Figure 5 shows the same type of data analysis for the S-wave signal as in Figure 4, and Figures 6 and 7 show the raw P- and S-wave signals used in Figures 4 and 5, respectively.

Figure 8 shows the P-wave signal collected in an iron sulfide sample before, during, and after a phase transition at high pressure. Panel (a) shows that the signals were lined up so that their buffer rod reflections were matched to show more clearly

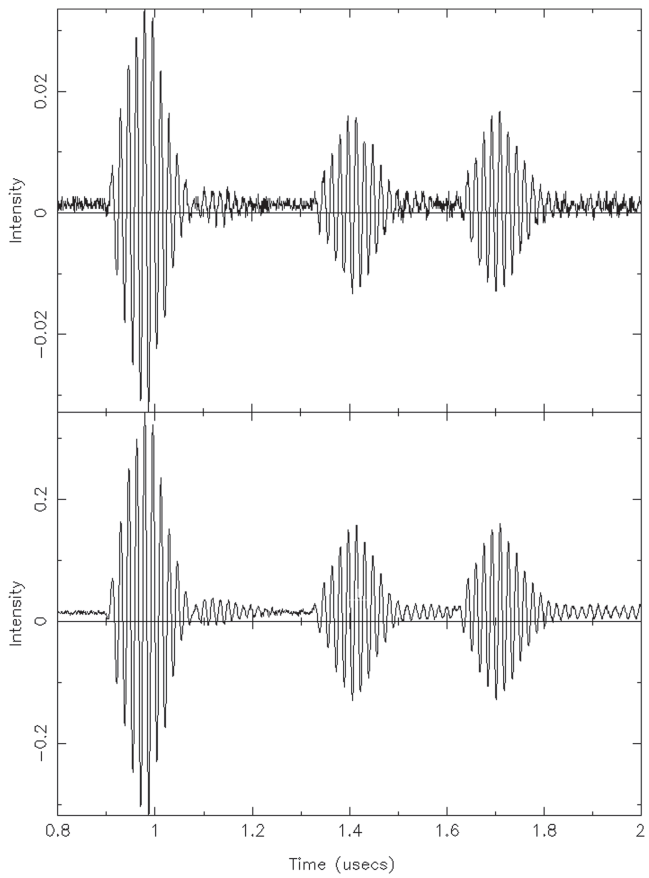

FIG. 6. The raw P-wave signal at 62 MHz, 5 cycles. The panels are organized as in Figure 4.

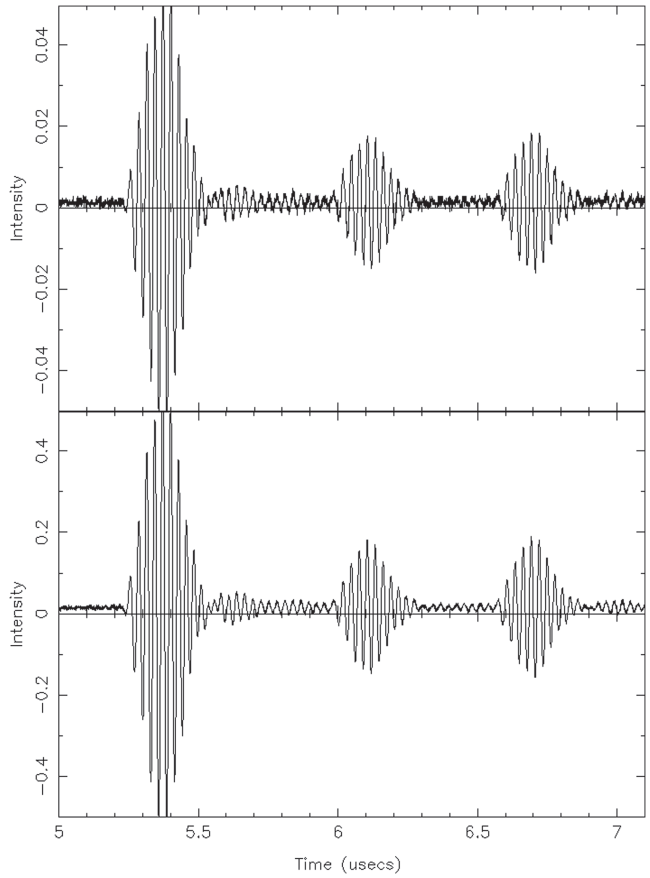

FIG. 7. The raw S-wave signal at 35 MHz, 5 cycles. The panels are organized as in Figure 4.

the changes in the travel time in the sample itself. Panel (b) is a blow up of panel (a), showing only the sample reflection signal for clarity. The sample was compressed to a pressure of 8 GPa at room temperature, under which conditions the monoclinic FeS-III phase is stable. The P-wave signal collected under these conditions is shown in dark gray. Then, the sample was rapidly heated to 200 °C to cross into the stability field of the hexagonal FeS-IV phase. Immediately upon reaching the desired temperature, while the phase transition was actively occurring, the P-wave signal was collected again, as shown in light gray. The temperature was then held constant for 200 s to allow the phase transition to come to completion while the P-wave signal was collected every 5 s up to 180 s. The signal at 5 s is nearly identical to that at 1 s, but by 10 s the signal begins to shift toward the final position shown in black. The final travel time position shown in black was reached by 40 s and remained constant through 180 s. The representative black signal shown in Figure 8 was collected at 60 s, and signals collected after longer time delays were identical to the 60 s signal, so they are not shown here.

Figure 8 shows quite clearly that the P-wave travel times are longer in the FeS-IV phase than in the FeS-III phase. Moreover, the travel times are even longer while this phase transition is taking place than when either phase is the sole stable structure, as is shown by the shift of the light gray signal to the right of the other two. Previously existing systems for ultrasonic velocity measurements at high pressures that take on the order of ~180 s to collect data would have easily been able to collect data on the FeS-III (dark gray) and FeS-IV (black) phases. However, their prohibitively long data collection times means that the increase in travel time that is observed while the phase transition is actively occurring would be lost

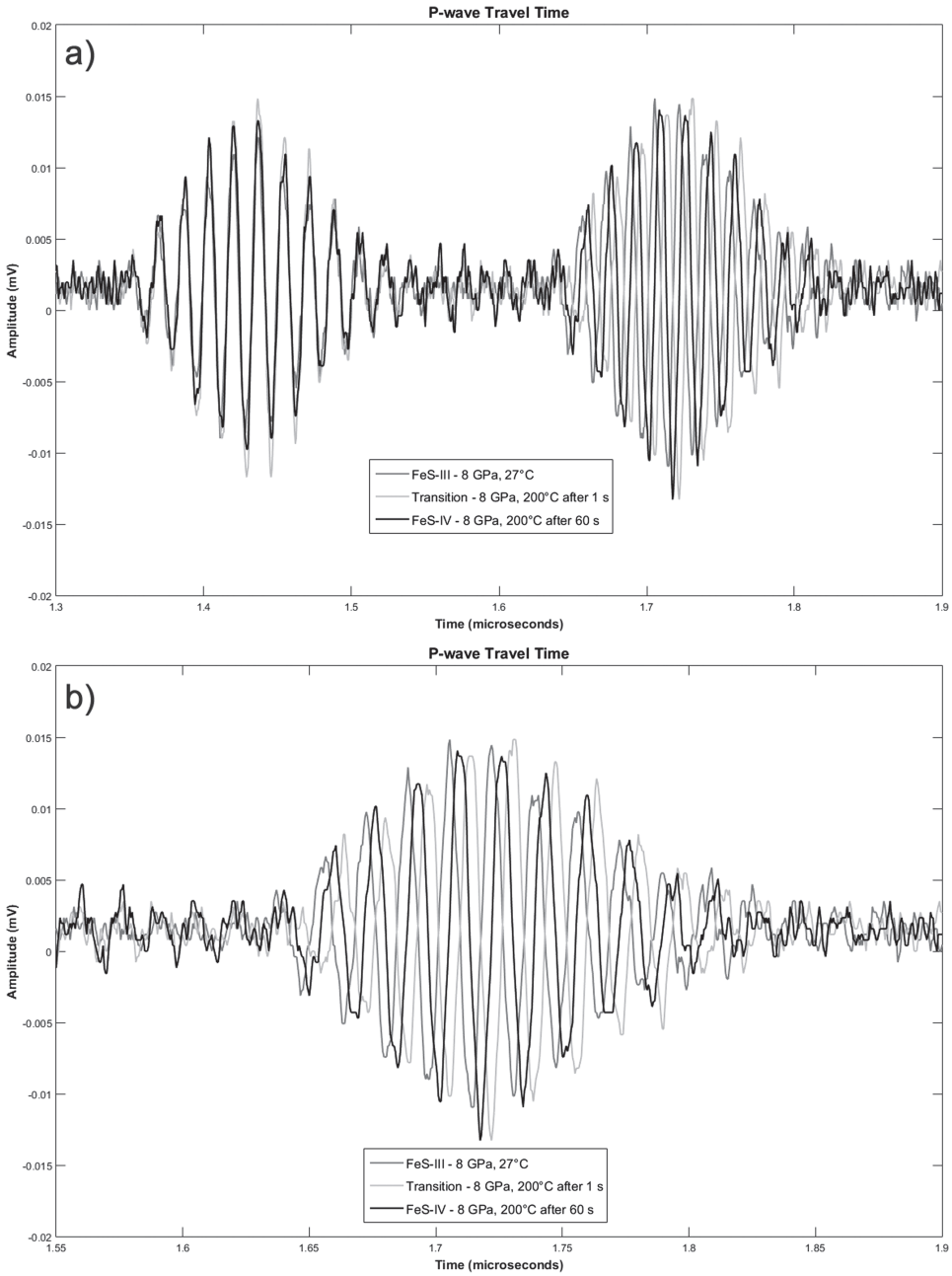

FIG. 8. P-wave signal collected in the FeS sample bracketing phase transition at 8 GPa. Shown in dark gray is FeS-III phase collected at room temperature. In light gray is the signal collected immediately upon reaching 200 °C while phase transition is actively occurring. Black line is the signal collected at 200 °C after 60 s when transition to FeS-IV is complete. Signals are normalized to buffer rod reflection time to show travel time differences. (a) Buffer rod and sample reflections shown. (b) Zoom in on sample signal to show differences in travel time.

and averaged into the longer-term stable signal of the single phase end products. It is important to note that in such a circumstance, nearly 25% of the acquisitions would be collected before the phase transition had completed, and their averaging with the rest of the acquisitions collected following the completion of the phase transition may have an effect on the signal position and quality. Moreover, existing systems that are capable of collecting data on the order of 30 s would have missed both the extreme slowing of the travel time associated with the onset of the phase transition and the travel time of the final phase after the transition was completed, which did not occur until ~40 s after the temperature change, instead yielding an averaged signal that does not represent the transient state or the final state. The increased data collection speed of the DIASCoPE system allows us for the first time to be able to observe such transient properties, which will in turn begin to allow us to better determine exactly what effects these transient processes have on the physical properties of materials.

The DIASCoPE system has two major important implications. First, since we can collect the acoustic data on such a significantly shorter time scale than before (Figure 4, top), we can use DIASCoPE to directly probe the effects of transient processes. In other systems where the data are summed over a period of 30+ s, any transient effect that would occur on shorter time scales (i.e., melting, phase transitions, etc.) would be effectively lost in the data and dominated by the more steady-state products that result from these processes. Being able to collect data so quickly will allow us to observe the effects of these processes in real time as they occur rather than measuring only the properties of the end products that are produced by these processes. Second, in experimental protocols where time is not as much of a critical element, data can be collected over longer periods of time and the resulting data output will have significantly improved statistical quality when compared with the data output of other systems (Figure 4, bottom) which lends itself to greater confidence in the results obtained from these experiments.

V. CONCLUSION

We present here a new system for fast collection of acoustic wave velocity data in materials at high pressures in a multi-anvil apparatus. This new system, dubbed DIASCoPE, is capable of collecting ultrasonic interferometry data in 1 s or less, cutting this data collection time by over 1-2 orders of magnitude. The data obtained from DIASCoPE in 1 s are shown to be as robust as those obtained in existing ultrasonic experimental systems that sum their data acquisitions over much longer time scales. This allows for both the study of transient processes and increased statistical robustness of the data output collected over extended time scales similar to those employed by other systems. DIASCoPE represents a major step forward in acoustic velocity data collection time reduction that will finally allow us to begin to witness what effects various processes may have on the physical properties of materials at extreme conditions as they occur rather than focusing only on the products resulting from these processes.

ACKNOWLEDGMENTS

The authors would like to thank Michael T. Vaughan and Donald J. Weidner for their invaluable insights and Haiyan Chen for logistical assistance at the beamline. The authors gratefully acknowledge the helpful and constructive reviews of three anonymous reviewers and the helpful guidance of Associate Editor Chin-Tu Chen. Portions of this research were supported by NSF Grant No. EAR1361463 to DJW. Use of the Advanced Photon Source, Argonne National Laboratory, was supported by the U.S. Department of Energy, Office of Science, Office of Basic Energy Sciences, under Contract No. DE-AC02-06CH11357. Use of the 6-BM-B beamline was supported by COMPRES, the Consortium for Materials Properties Research in Earth Sciences, under NSF Cooperative Agreement No. EAR 01-35554 and by the Mineral Physics Institute, Stony Brook University. MPI Publication No. 508.

[1]B. S. Li and R. C. Liebermann, Proc. Natl. Acad. Sci. U. S. A. **104**(22), 9145–9150 (2007).
[2]B. S. Li and R. C. Liebermann, Phys. Earth Planet. Inter. **233**, 135–153 (2014).
[3]F. Birch, J. Geophys. Res. **65**(4), 1083–1102, doi:10.1029/jz065i004p01083 (1960).
[4]F. Birch, J. Geophys. Res. **66**(7), 2199, doi:10.1029/jz066i007p02199 (1961).
[5]G. L. Chen, R. C. Liebermann, and D. J. Weidner, Science **280**(5371), 1913–1916 (1998).
[6]L. M. Flesch, B. S. Li, and R. C. Liebermann, Am. Mineral. **83**(5-6), 444–450 (1998).
[7]H. Fujisawa, J. Geophys. Res.: Solid Earth **103**(B5), 9591–9608, doi:10.1029/98jb00024 (1998).
[8]H. Fujisawa, E. Ito, O. Ohtaka, and T. Yamanaka, Geophys. Res. Lett. **21**(14), 1499–1502, doi:10.1029/94gl01013 (1994).
[9]B. S. Li, I. Jackson, T. Gasparik, and R. C. Liebermann, Phys. Earth Planet. Inter. **98**(1-2), 79–91 (1996).
[10]B. S. Li, R. C. Liebermann, and D. J. Weidner, Science **281**(5377), 675–677 (1998).
[11]A. Yoneda, J. Phys. Earth **38**(1), 19–55 (1990).
[12]B. S. Li, J. Kung, and R. C. Liebermann, Phys. Earth Planet. Inter. **143**, 559–574 (2004).
[13]Y. Higo, Y. Kono, T. Inoue, T. Irifune, and K.-i. Funakoshi, J. Synchrotron Radiat. **16**, 762–768 (2009).
[14]Y. Kono, A. Yamada, Y. Wang, T. Yu, and T. Inoue, Rev. Sci. Instrum. **82**(2), 023906 (2011).
[15]Y. Wang, M. Rivers, S. Sutton, N. Nishiyama, T. Uchida, and T. Sanehira, Phys. Earth Planet. Inter. **174**(1-4), 270–281 (2009).
[16]J. Kung, B. S. Li, and R. C. Liebermann, J. Phys. Chem. Solids **67**(9-10), 2051–2055 (2006).
[17]M. L. Whitaker, W. Liu, Q. Liu, L. Wang, and B. Li, High Pressure Res. **28**(3), 385–395 (2008).
[18]T. Irifune, Y. Higo, T. Inoue, Y. Kono, H. Ohfuji, and K. Funakoshi, Nature **451**(7180), 814–817 (2008).
[19]M. L. Whitaker, W. Liu, Q. Liu, L. Wang, and B. Li, Am. Mineral. **94**(7), 1039–1044 (2009).
[20]W. Liu, Q. Liu, M. L. Whitaker, Y. Zhao, and B. Li, J. Appl. Phys. **106**, 043506 (2009).
[21]M. L. Whitaker, W. Liu, L. Wang, and B. Li, J. Earth Sci. **21**(5), 792–800 (2010).
[22]Q. Liu, W. Liu, M. L. Whitaker, L. Wang, and B. Li, Am. Mineral. **95**(7), 1000–1005 (2010).
[23]Y. Kono, T. Irifune, Y. Higo, T. Inoue, and A. Barnhoorn, Phys. Earth Planet. Inter. **183**(1-2), 196–211 (2010).
[24]Y. Zou, T. Irifune, S. Greaux, M. L. Whitaker, T. Shinmei, H. Ohfuji, R. Negishi, and Y. Higo, J. Appl. Phys. **112**(1), 014910 (2012).
[25]Y. Kono, C. Park, C. Kenney-Benson, G. Shen, and Y. Wang, Phys. Earth Planet. Inter. **228**, 269–280 (2014).
[26]B. S. Li, J. Kung, W. Liu, and R. C. Liebermann, Phys. Earth Planet. Inter. **228**, 63–74 (2014).

[27]X. Wang, T. Chen, X. Qi, Y. Zou, J. Kung, T. Yu, Y. Wang, R. C. Liebermann, and B. Li, J. Appl. Phys. **118**(6), 065901 (2015).
[28]J. Chantel, G. M. Manthilake, D. J. Frost, C. Beyer, T. B. Ballaran, Z. Jing, and Y. Wang, Am. Mineral. **101**(4), 991–997 (2016).
[29]S. Greaux, Y. Kono, Y. B. Wang, A. Yamada, C. Y. Zhou, Z. C. Jing, T. Inoue, Y. Higo, T. Irifune, N. Sakamoto, and H. Yurimoto, Geophys. Res. Lett. **43**(9), 4239–4246, doi:10.1002/2016gl068377 (2016).
[30]A. Yokoyama, M. Matsui, Y. Higo, Y. Kono, T. Irifune, and K. Funakoshi, J. Appl. Phys. **107**(12), 123530 (2010).
[31]O. L. Anderson, D. G. Isaak, and S. Yamamoto, J. Appl. Phys. **65**(4), 1534–1543 (1989).
[32]D. L. Decker, J. Appl. Phys. **42**(8), 3239 (1971).
[33]G. F. Davies and A. M. Dziewonski, Phys. Earth Planet. Inter. **10**(4), 336–343 (1975).